analytical chemistry

pubs.acs.org/ac Article

Deep Learning-Based Sensor Array: 3D Fluorescence Spectra of Gold Nanoclusters for Qualitative and Quantitative Analysis of Vitamin B_6 Derivatives

Hamada A. A. Noreldeen, Kai-Yuan Huang, Gang-Wei Wu, Hua-Ping Peng, Hao-Hua Deng,* and Wei Chen*

Cite This: *Anal. Chem.* 2022, 94, 9287−9296 Read Online

ACCESS | Metrics & More | Article Recommendations | Supporting Information

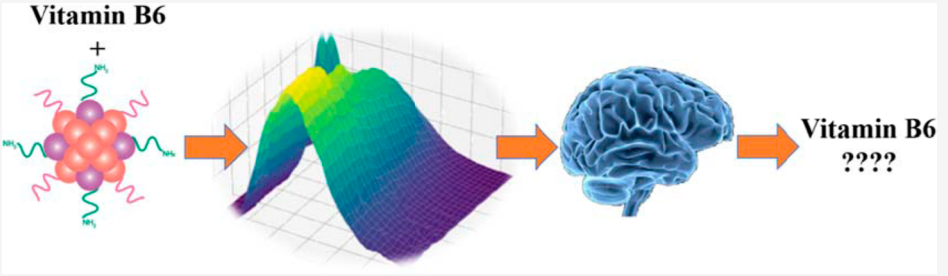

ABSTRACT: Vitamin B_6 derivatives (VB6Ds) are of great importance for all living organisms to complete their physiological processes. However, their excess in the body can cause serious problems. What is more, the qualitative and quantitative analysis of different VB6Ds may present significant challenges due to the high similarity of their chemical structures. Also, the transfer of deep learning model from one task to a similar task needs to be present more in the fluorescence-based biosensor. Therefore, to address these problems, two deep learning models based on the intrinsic fingerprint of 3D fluorescence spectra have been developed to identify five VB6Ds. The accuracy ranges of a deep neural network (DNN) and a convolutional neural network (CNN) were 94.44−97.77% and 97.77−100%, respectively. After that, the developed models were transferred for quantitative analysis of the selected VB6Ds at a broad concentration range (1−100 μM). The determination coefficient (R^2) values of the test set for DNN and CNN were 93.28 and 97.01%, respectively, which also represents the outperformance of CNN over DNN. Therefore, our approach opens new avenues for qualitative and quantitative sensing of small molecules, which will enrich fields related to deep learning, analytical chemistry, and especially sensor array chemistry.

INTRODUCTION

Vitamin B_6 is one of the most important organic cofactors for a large number of enzymes for all organisms (eukaryotic and prokaryotic).[1] In addition to its important role in enzymatic processes such as fatty acid and amino acid metabolism,[2−4] it inhibits reactive oxygen species, and it is regarded as a potential fungal antioxidant.[5] Hence, all organisms need vitamin B_6, and they have to synthesize it or obtain it from food.[5] Also, a high intake of vitamin B_6 in the diet was associated with a lower risk of death from stroke, coronary heart disease, and heart failure.[4] In contrast, a low intake of vitamin B_6 was associated with a higher risk of colorectal cancer.[6] Vitamin B_6 intake also has a significant effect on modulating some parameters of the colon, including several gene expressions and several free amino acids.[7] On the other hand, other researchers have indicated that very high doses of vitamin B_6 (≥200 mg/kg) can cause several problems in the nerve system, including the loss of body control (ataxia), peripheral nerve damage,[8] and damage of sensory fibers in peripheral nerves, which is hard to return to normal after treatment.[9,10] Furthermore, it can affect reproductive health. For instance, pyridoxine at 0.5 or 1 g/kg is associated with a decrease in the formation and motility of sperms. Also, the weight and the histology of the testes can be changed.[11,12] It is important to note that the normal daily allowance of vitamin B_6 for adults is approximately between 1 and 2 mg.[13] Of note, the derivatives of vitamin B_6 include pyridoxine, pyridoxal, pyridoxamine, pyridoxal 5′-phosphate, and pyridoxamine 5′-phosphate.[1,14] Pyridoxine and phosphorylated derivatives are considered the main dietary forms of VB6Ds.[15] Pyridoxal 5′-phosphate is regarded as a biologically active form of VB6Ds and participates in many enzymatic reactions. Pyridoxamine is a minor form of VB_6, which only—among all other VB6Ds—can deactivate

Received: February 9, 2022
Accepted: June 9, 2022
Published: June 18, 2022

https://doi.org/10.1021/acs.analchem.2c00655
Anal. Chem. 2022, 94, 9287−9296

Scheme 1. Schematic Illustration of the Deep Learning-Based Fluorescence Sensor Array for Qualitative and Quantitative Analysis of VB6Ds

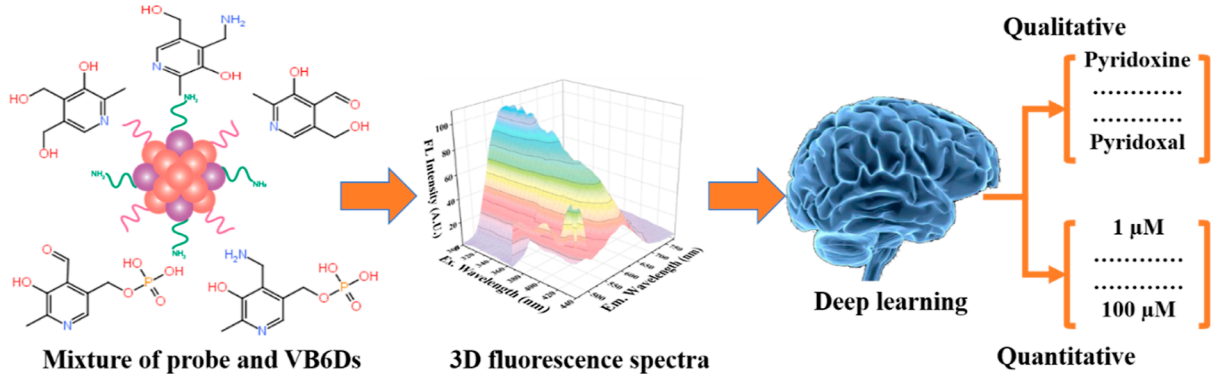

advanced glycation end product formation.[14] Also, it is found to correlate with other diseases, including obesity, endothelial dysfunction, and kidney dysfunction.[14] However, to the best of our knowledge, to date, there is no publication for the qualitative and quantitative analysis of vitamin B_6 derivatives (VB6Ds) based on the sensor array.

Recently, gold nanoclusters (AuNCs) have been used in the field of sensing construction due to their advantages, which include their stability, ease of preparation, large Stokes shift, and low toxicity. Therefore, such advantages could qualify them for medical and environmental uses.[16,17] These applications include protein detection, biomarker identification and monitoring, biological imaging, drug and small molecule detection, heavy metal ion detection, bacteria identification, and others.[16−24] Despite the different uses of AuNCs, they are used for sensing in a lock-and-key method (one receptor for one target). Therefore, this method is not suitable for identifying more than one target with similar chemical structures. Accordingly, using the sensor array that simulates smell and taste in humans may be the best choice to differentiate between more than one target. The sensor array approach is based on the collection of multiple responses for each target, which facilitates the identification of each target.[25−27] The dependence of this approach on the analysis of different response patterns rather than specific interactions between receptors and targets is regarded as one of its most important advantages.[28] However, many publications based on this approach used several probes for collecting differentiable response patterns as much as possible to differentiate different analysts,[29,30] which increases the workload and the cost. Therefore, a simple, stable, and sensitive detection approach using AuNCs as a single probe for sensor array construction to identify and quantify different analytes with similar chemical structures is highly needed.

Artificial intelligence currently represents a new way to solve problems related to scientific research.[21,31] Deep learning is one of the most important branches of artificial intelligence that is used in many research fields.[32−35] Deep learning includes advanced algorithms that can find complex relationships in complex environments, which traditional algorithms might not.[21,35] The combination of deep learning with analytical chemistry led to a great development, which demonstrated the power of deep learning to analyze images of cancer patients.[36−38] The deep neural network (DNN)-based surface-enhanced Raman spectrometry has also been used to differentiate between cancer suppression genes with an accuracy of 90%.[39] A convolutional neural network (CNN) was also used for spectrum analysis, as it was used to predict the concentrations of mixtures of amino acids with a determination coefficient of 99%.[40] It is worth noting that CNN is one of the most important deep learning algorithms, and therefore, it has been used in many bio-analytical analysis tasks.[41] Also, Lu *et al.* used CNN to identify single microbial cells with 95% accuracy.[42] What is more, CNN is less dependent on the preprocessing step as in the other chemometric approaches,[35] where CNN automatically extracts features.[32] Moreover, CNN uses convolution operators, which enables it to solve problems with high computational costs, as in the case of classifying a large number of images with different quality.[32] Furthermore, in convolutional layers, kernels are used to produce feature mapping. Including these layers will reduce parameters (so-called weight sharing) and will make these layers learn correlations from neighboring pixels (so-called local connectivity).[32,43] What is more, transferability is regarded as one of the most important characteristics of CNN.[44] Transfer learning means training the model to solve a problem and then re-using it in another similar problem, which means that the new problem can be solved with the least possible data set.[45] Although transfer learning has been used in the medical field,[44,45] it did not get much attention in the fluorescence-based biosensor field.

Furthermore, our previous study presented a fluorescence quenching effect that has been found due to the interaction of cysteamine/*N*-acetyl-L-cysteine/AuNCs (Cys/NAC−AuNCs) and pyridoxal phosphate (PLP) through the photoinduced electron transfer (PET) mechanism.[46] Therefore, depending on this phenomenon, we hypothesized that different VB6Ds could be identified. Inspired by all of these studies, in our study, a deep learning approach-based sensor array has been developed for the qualitative analysis of five VB6Ds. First, a Cys/NAC−AuNCs solution was used as a single probe, and 3D fluorescence data resulting from the interaction of the probe and different VB6Ds was used as input data. The 3D fluorescence data was used as a full fingerprint to cover as many distinct emission and excitation regions as possible due to the interaction between the receptor and targets. Next, DNN and CNN were selected for our study, and several classification metrics were used to evaluate and compare our models. After that, the established models were transferred to quantify the selected VB6Ds at nine concentrations, and several prediction metrics were used to evaluate and compare our models. To the best of our knowledge, this is the first study to identify and quantify the different VB6Ds based on a fluorescence sensor array. Scheme 1 shows the general procedures of our approach.

https://doi.org/10.1021/acs.analchem.2c00655
Anal. Chem. 2022, 94, 9287−9296

EXPERIMENTAL SECTION

Deep Learning Model Building and Optimization. The data set was split randomly into three sets: training, validation, and test set (6:2:2, respectively). The training set was used to perform the actual training for our model, while the validation set was used for the fine-tuning of the model hyperparameter after each epoch, which let the model reach the optimal performance. Accordingly, the test set was used to report the final model accuracy. For the training process, DNN and CNN were separately employed (Figure S2). The Keras and Tensorflow, Python deep-learning libraries, were used in our study. First, in the case of qualitative analysis, DNN and CNN both consist of five layers, including one input layer, three hidden layers, and one output layer (Figure S2). It is important to know that the batch size and the activation function of the hidden layers were tuned using GridSearchCV. Furthermore, fivefold cross-validation was applied to overcome the chance of overfitting, reduce the high sensitivity for a particular data point, and reduce the high sensitivity for a specific class as much as possible. Also, it is useful for checking how well the models could perform on a new data set.[47] It is worth mentioning that in the fivefold cross-validation step, the training set was divided into five parts, and each time the data used one part as a test set and the rest as a train set, then repeated the process 5 times so that the test set can cover all parts. After that, the models were trained repeatedly for 100 epochs. Then, the relationship between the loss/accuracy values and epochs' number was monitored to select the optimized epoch number according to the minimal value of the validation loss.

Second, the transfer learning approach was applied for the quantitative analysis. The number of layers, activation function of hidden layers, and batch size were used in the same manner as the qualitative analysis (Figure S3). What is more, the models were trained repeatedly for 10,000 epochs, and the epoch number was monitored in the same manner as the qualitative analysis. Of note, sparse categorical cross-entropy was applied as a loss function to train the deep learning models in the qualitative analysis. However, mean squared error was used as a loss function to train the deep learning models in the quantitative analysis. Also, Adam was used as the optimizer for the qualitative and quantitative analyses.

Deep Learning Model Evaluation. In the case of the qualitative analysis, the models' results were evaluated using accuracy, precision, recall, and F1 score. The classifier precision was regarded as the accuracy of the positive predictions. The precision was usually used with recall (also called sensitivity or the true positive rate), which means the corrected positive ratio that was detected using a classifier. F1 score is regarded as a combination of precision and recall. It is usually used in classification as a simple way to compare multi-classifiers. F1 score is also regarded as a harmonic mean of precision and recall. Thus, the F1 score grants more weight to lower values, which is opposite to the normal mean that treats all values equally. Therefore, the F1 score will be high only in the case when precision and recall will have high values.[48]

$$\text{Accuracy} = \frac{(\text{TP} + \text{TN})}{(\text{TP} + \text{TN} + \text{FP} + \text{FN})} \tag{1}$$

$$\text{Precision} = \frac{\text{TP}}{(\text{TP} + \text{FP})} \tag{2}$$

$$\text{Recall} = \frac{\text{TP}}{(\text{TP} + \text{FN})} \tag{3}$$

$$\text{F1 score} = 2 \times \frac{\text{precision} \times \text{recall}}{\text{precision} + \text{recall}} \tag{4}$$

where TP and TN are equal to the number of true positive and true negative, respectively. Also, FP and FN represent the number of false positives and false negatives, respectively.

On the other hand, for the quantitative analysis, the models' results were evaluated using mean square error (MSE), root MSE (RMSE), mean absolute error (MAE), median absolute error (MedAE), and determination coefficient (R^2).[49] RMSE expresses the amount of error committed by the model during the predictions task,[48] and it is the square root of MSE as present in the following equations.[50] MAE is similar to RMSE; however, it is less sensitive to outliers than RMSE.[48] MAE and RMSE are also called L1 and L2 distances, respectively.[51] MedAE is very important because it is robust in the case of outliers. It is the average of all the absolute differences between the real and expected values.[52] R^2 measures the amount of variance in concentrations (dependent variables) that can be forecasted from fluorescence spectra (independent variables).[53] Thus, R^2 is useful to predict the applicability of the models for unseen data (test set as an example).

$$\text{MSE} = \frac{1}{m}\sum_{i=0}^{m-1}(y_{(i)} - \hat{y}_{(i)})^2 \tag{5}$$

$$\text{RMSE} = \sqrt{\frac{1}{m}\sum_{i=0}^{m-1}(y_{(i)} - \hat{y}_{(i)})^2} \tag{6}$$

$$\text{MAE} = \frac{1}{m}\sum_{i=0}^{m-1}|y_{(i)} - \hat{y}_{(i)}| \tag{7}$$

$$\text{MedAE} = \text{median}(|y_1 - \hat{y}_1|, \ldots, |y_n - \hat{y}_n|) \tag{8}$$

$$R^2 = 1 - \frac{\sum_{i=1}^{m}(y_{(i)} - \hat{y}_{(i)})^2}{\sum_{i=1}^{m}(y_{(i)} - \bar{y})^2} \tag{9}$$

where

$$\bar{y} = \frac{1}{m}\sum_{i=1}^{m} y_{(i)} \tag{10}$$

where m represents the number of samples, and y_i and $\hat{y}_i$ are actual and predicted values of the ith sample, respectively. Also, $\bar{y}$ represents the mean of the actual values.

RESULTS AND DISCUSSION

Characterization and Modulation of the Fluorescence of the Sensor Array Probe. Our previous study indicated that the quenching effect was shown in the fluorescence of Cys/NAC−AuNCs due to the interaction of Cys/NAC−AuNCs and different concentrations of pyridoxal 5′-phosphate (PLP). This effect resulted from the PET mechanism.[46] Therefore, in this study, Cys/NAC−AuNCs solution has been prepared and used as a single probe for the qualitative and quantitative analysis of five VB6Ds based on the different 3D fluorescence spectra resulting from the interactions between the Cys/NAC−AuNCs and the individual VB6Ds. Of note, the five VB6Ds are pyridoxine, pyridoxal, pyridoxamine, pyridoxal 5′-phosphate,

https://doi.org/10.1021/acs.analchem.2c00655
Anal. Chem. 2022, 94, 9287−9296

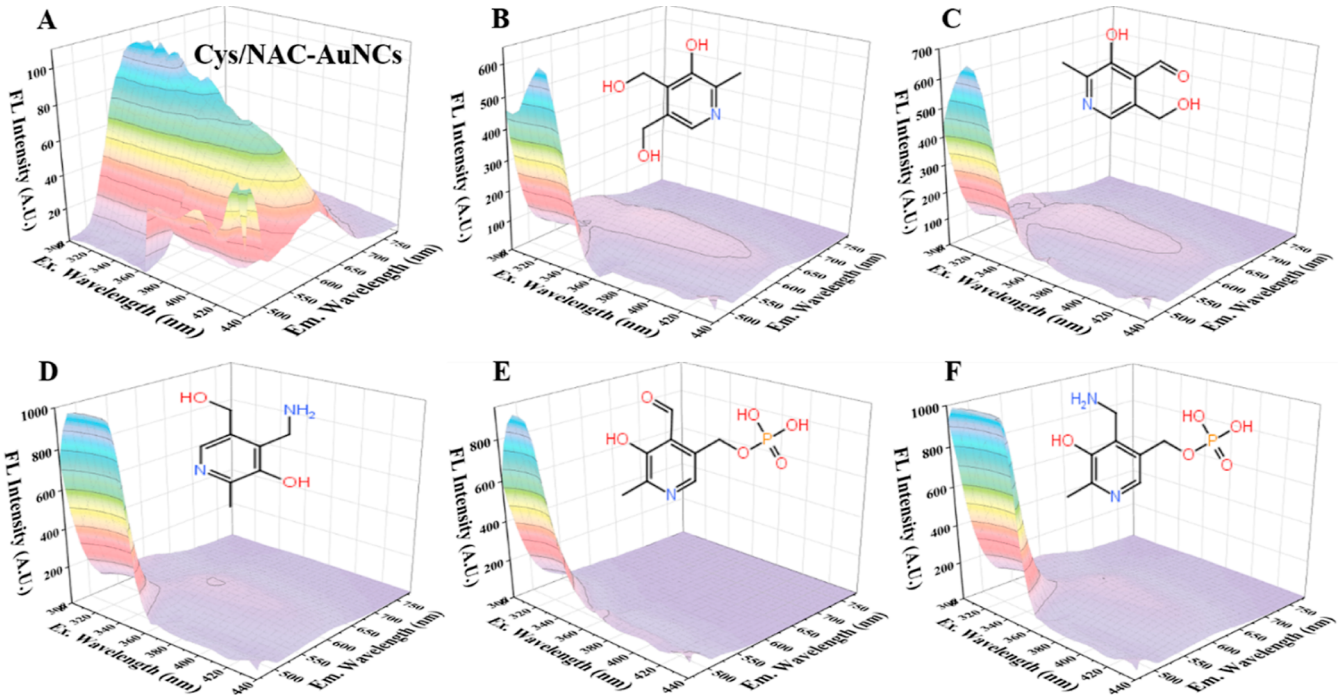

Figure 1. 3D fluorescence spectra of (A) Cys/NAC−AuNC and the mixture of Cys/NAC−AuNC with (B) pyridoxine, (C) pyridoxal, (D) pyridoxamine, (E) pyridoxal 5′-phosphate, and (F) pyridoxamine 5′-phosphate at 100 μM.

and pyridoxamine 5′-phosphate. Accordingly, the synthesis of Cys/NAC−AuNCs was proved by transmission electron microscopy. Figure S4 exhibits that Cys/NAC−AuNCs were mono-dispersed spheres.

Figure 1 presents different 3D fluorescence spectra resulting from mixing Cys/NAC−AuNCs with five VB6Ds individually. We can realize the notable differences between the 3D fluorescence spectra of the probe (Figure 1A) and the 3D fluorescence spectra resulting from the interaction of the probe and different VB6Ds (Figure 1B−F). These differences may be resulting from the different functional groups of the target molecules.[54] Although there are similarities in function groups that result in the production of similar 3D fluorescence spectra of different VB6Ds, there are also differences in fluorescence intensity, especially at the beginning of the excitation range (300−350 nm), as shown in Figure 1B−F. In general, there are apparent fluctuation effects in the fluorescence spectra of Cys/NAC−AuNCs as a result of adding different VB6Ds. These effects are also noted when comparing the fluorescence spectra of different VB6Ds at 600 nm under an excitation wavelength of 425 nm, as shown in Figure S5.

Figure S5 clearly shows the presence of two characteristic regions that fluorescence spectra change across: region 1 (470−510 nm) and region 2 (510−750 nm). Of note, region 2 is characteristic of fluorescence spectra of Cys/NAC−AuNCs.[46] As seen, the mixture of probe−pyridoxal 5′-phosphate has an obvious enhancement effect and obvious quenching effect in regions 1 and 2, respectively. However, the mixture of probe−pyridoxamine 5′-phosphate has quenching effects across the two regions. On the other hand, the mixture of probe−pyridoxine, probe−pyridoxal, and probe−pyridoxamine shows a few enhancement effects. Also, the mixture of probe−pyridoxine and probe−pyridoxal has almost the same fluorescence spectra. Therefore, we assume that using the entire fingerprint fluorescence spectrum (3D fluorescence spectra), including all its distinct spectral regions, can help us identify very similar compounds. Also, the use of deep learning algorithms can help in the identification of similar compounds by extracting distinct information for each VB6Ds.

Deep Learning Model Optimization and Selection of Optimal Hyperparameter. As we mentioned above, DNN and CNN have been used for the qualitative analysis. First, for getting models with optimal parameters and hyperparameters, Adam has been selected as an optimizer in our study, where it is considered the best optimizer in spectral analysis.[34,35,55−58] Also, sparse categorical cross-entropy,[59] accuracy, and softmax[38] have been considered as the loss function, metrics, and activation function of the output layer, respectively. After that, the DNN and CNN having five layers were constructed and considered for our purpose (Figure S2). Subsequently, the constructed models with GridSearchCV were considered to find the rest of the hyperparameters, namely, batch size and activation function of the hidden layers. Accordingly, our result revealed that the best accuracy of the DNN model was achieved when the activation was linear and the batch size was 16. While the best accuracy of the CNN model was achieved when the activation was Rectified Linear Unit (ReLU) and the batch size was 32. Of note, the equations of linear and ReLU are "$f(x) = x$" and "$f(x) = \max(0, x)$", respectively.[60] Therefore, these hyperparameters have been considered in the rest of our study.

$$\text{Cross-entropy} = -\frac{1}{m}\sum_{i=1}^{m}[y_{(i)}\ln(\hat{y}_{(i)}) + (1 - y_{(i)})\ln(1 - \hat{y}_{(i)})] \quad (11)$$

$$\text{Softmax}(f(z_i)) = \frac{e^{x_i}}{\sum_{j=1}^{m} e^{x_j}} \quad (12)$$

where m represents the number of samples; y_i and $\hat{y}_i$ are actual and predicted values of the ith sample, respectively; and $f(z_i)$ represents the output of the ith neuron.

https://doi.org/10.1021/acs.analchem.2c00655
Anal. Chem. 2022, 94, 9287−9296

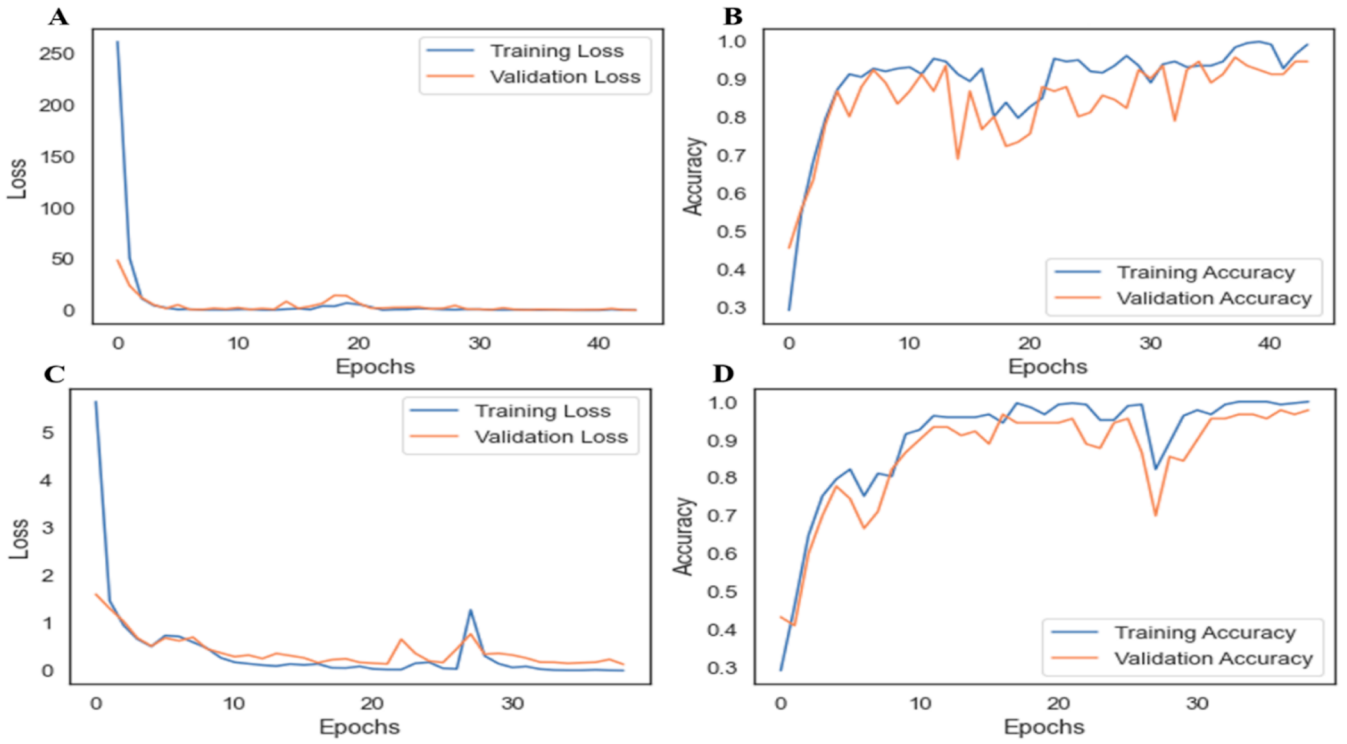

Figure 2. Convergence curves during the fine-tuning process in the models' training and validation at the selected epochs' number (44 and 39 for DNN and CNN, respectively). (A,B) Loss and accuracy of DNN, respectively. (C,D) Loss and accuracy of CNN, respectively.

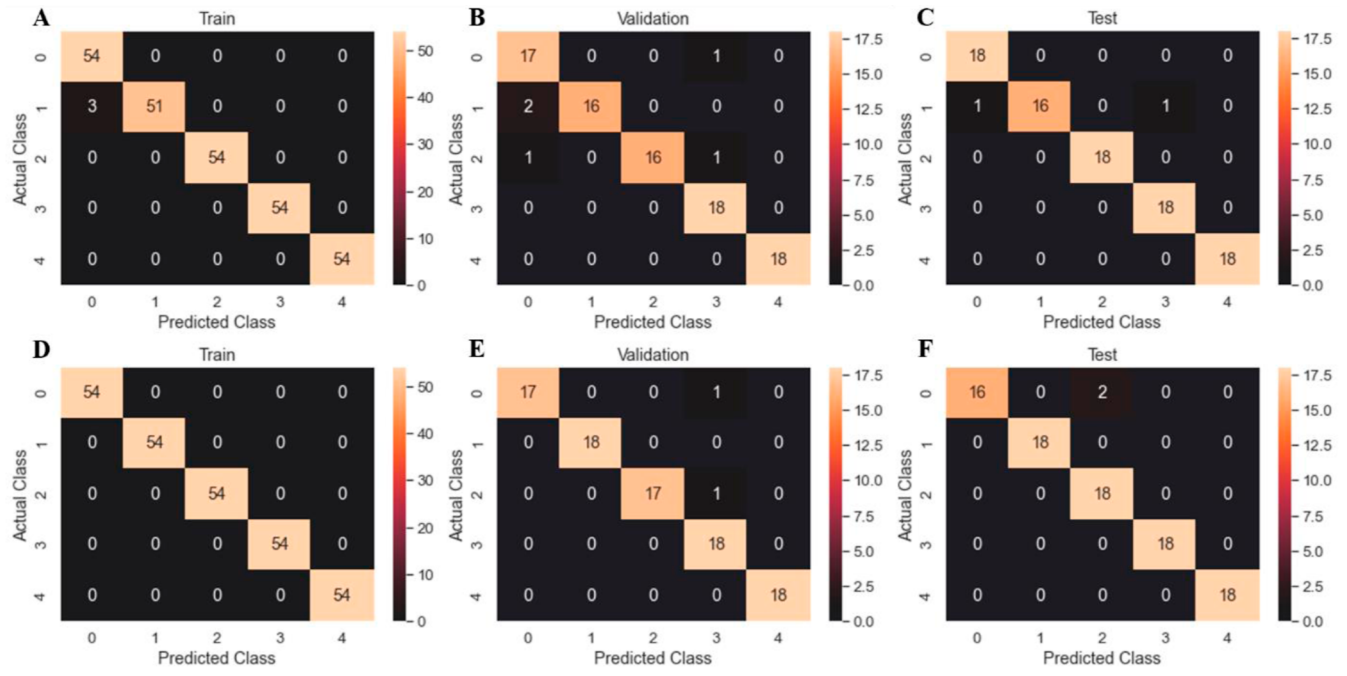

Figure 3. (A−C) Confusion matrix of DNN for the train, test, and validation set, respectively. (D−F) Confusion matrix of CNN for the train, test, and validation set, respectively. Samples marked as 0−4 correspond to pyridoxine, pyridoxal, pyridoxamine, pyridoxal 5′-phosphate, and pyridoxamine 5′-phosphate, respectively.

Deep Learning Models for Qualitative Analysis of Vitamin B_6 Derivatives. The loss function of DNN and CNN converged in the training process at 100 epochs (Figure S6). Also, the best results have been considered according to the lowest value of the validation loss. Accordingly, Figure 2 represents the best result found at 44 and 39 epochs for DNN and CNN, respectively. Furthermore, the performances of DNN and CNN have been presented in Figure 3. First, for the training set, there is an overlap between pyridoxine and pyridoxal in the case of DNN (Figure 3A). Three data points of pyridoxal have been identified as pyridoxine. These may be due to the high structural similarity between pyridoxine and pyridoxal. However, for CNN, no overlap has been seen (Figure 3D). Second, in the validation set of DNN, also, there are overlaps between

https://doi.org/10.1021/acs.analchem.2c00655
Anal. Chem. 2022, 94, 9287−9296

Table 1. Classification Report of DNN and CNN Models' Performance for the Qualitative Analysis of Five VB6Ds Using 3D Fluorescence Data

	train set (accuracy = 0.99)			validation set (accuracy = 0.94)			test set (accuracy = 0.98)		
DNN	precision	recall	F1 score	precision	recall	F1 score	precision	recall	F1 score
0[a]	0.95	1.00	0.97	0.85	0.94	0.89	0.95	1.00	0.97
1	1.00	0.94	0.97	1.00	0.89	0.94	1.00	0.89	0.94
2	1.00	1.00	1.00	1.00	0.89	0.94	1.00	1.00	1.00
3	1.00	1.00	1.00	0.90	1.00	0.95	0.95	1.00	0.97
4	1.00	1.00	1.00	1.00	1.00	1.00	1.00	1.00	1.00
macro-average	0.99	0.99	0.99	0.95	0.94	0.94	0.98	0.98	0.98
weighted average	0.99	0.99	0.99	0.95	0.94	0.94	0.98	0.98	0.98
	train set (accuracy = 1.00)			validation set (accuracy = 0.98)			test set (accuracy = 0.98)		
CNN	precision	recall	F1 score	precision	recall	F1 score	precision	recall	F1 score
0[a]	1.00	1.00	1.00	1.00	0.94	0.97	1.00	0.89	0.94
1	1.00	1.00	1.00	1.00	1.00	1.00	1.00	1.00	1.00
2	1.00	1.00	1.00	1.00	0.94	0.97	0.90	1.00	0.95
3	1.00	1.00	1.00	0.90	1.00	0.95	1.00	1.00	1.00
4	1.00	1.00	1.00	1.00	1.00	1.00	1.00	1.00	1.00
macro-average	1.00	1.00	1.00	0.98	0.98	0.98	0.98	0.98	0.98
weighted average	1.00	1.00	1.00	0.98	0.98	0.98	0.98	0.98	0.98

[a]Samples marked as 0−4 correspond to pyridoxine, pyridoxal, pyridoxamine, pyridoxal 5′-phosphate, and pyridoxamine 5′-phosphate, respectively.

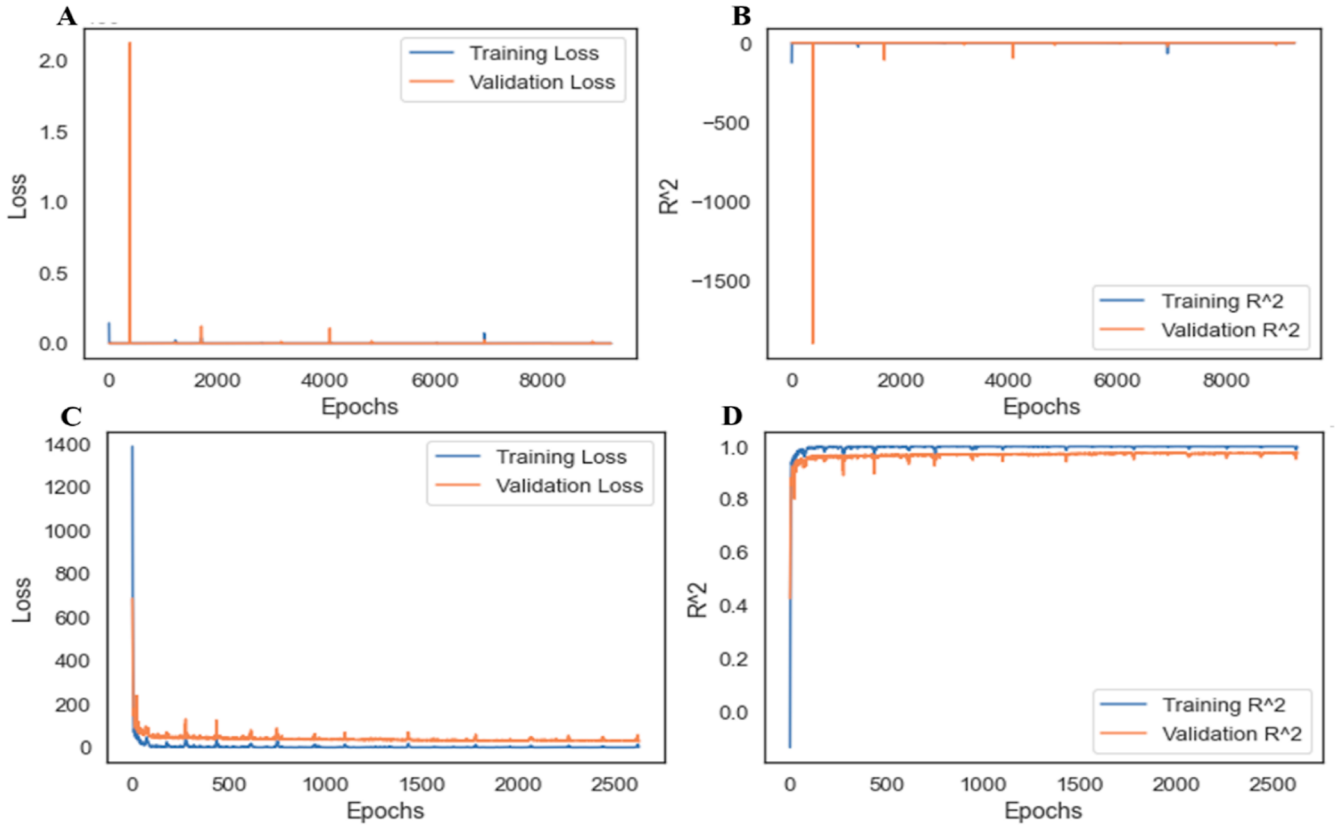

Figure 4. Convergence curves during the fine-tuning process in the models' training and validation at the selected epochs' number (9253 and 2622 for DNN and CNN, respectively). (A,B) Loss and determination coefficient (R^2) of DNN, respectively. (C,D) Loss and determination coefficient (R^2) of CNN, respectively.

pyridoxine and pyridoxal. Besides, there is a single overlap between pyridoxine and pyridoxamine. Also, the overlaps have been seen between pyridoxine and pyridoxal 5′-phosphate and between pyridoxamine and pyridoxal 5′-phosphate (Figure 3B). On the other hand, in the validation set of CNN, there are two overlaps between pyridoxine and pyridoxal 5′-phosphate and between pyridoxamine and pyridoxal 5′-phosphate (Figure 3E). Finally, the test set of DNN showed the overlaps between pyridoxine, pyridoxal, and pyridoxal 5′-phosphate. In contrast, the test set of CNN showed the overlaps between pyridoxine and pyridoxamine. All these overlaps are due to the strong similarity in chemical structures and functional groups of VB6Ds. Altogether, the performance of CNN is better than the performance of DNN in the qualitative analysis of VB6Ds.

https://doi.org/10.1021/acs.analchem.2c00655
Anal. Chem. 2022, 94, 9287−9296

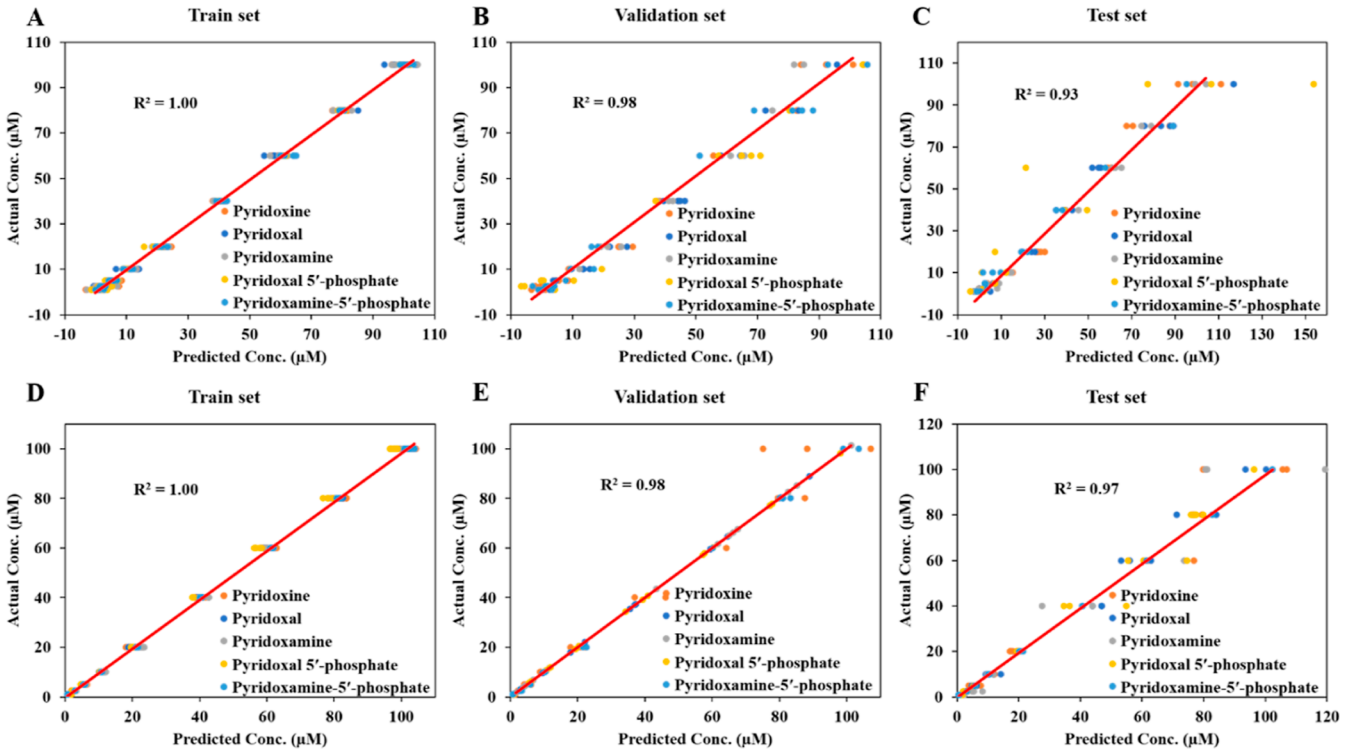

Figure 5. Quantitative analysis of five VB6Ds. (A−C) Predicted *vs* actual concentrations of the train, validation, and test set for the DNN model, respectively. (D−F) Predicted *vs* actual concentrations of the train, validation, and test set for the CNN model, respectively. R^2 is placed on the figure as an example to illustrate the overall performance of the models. More details about the data points of the test set can be seen in Table S1.

Additionally, DNN and CNN have been fully compared using a complete classification report, as shown in Table 1. As we mentioned above, the F1 score will have a high value when precision and recall have high values. Therefore, the precision and recall of the train set of DNN have values ≥95% (except the recall value of pyridoxal that equals 94.44%). Accordingly, the value of the F1 score is ≥97%. Turning to the train set of CNN, the precision and recall have values equal to 100%. Accordingly, the value of the F1 score is 100%. Therefore, the F1 score expresses the balance between precision and recall. This observation becomes clear in the validation set of DNN, where the values of precision and recall are 85 and 94.44%, respectively; accordingly, the F1 score is 89.47%. Also, the same concept can be applied to the rest values of the DNN model. At the same time, in the validation set of CNN, pyridoxine and pyridoxamine have the same precision and recall values of 100 and 94.44%, respectively; hence, the F1 score is equal to 97.14% for each. Furthermore, pyridoxal and pyridoxamine 5′-phosphate have the same precision and recall values of 100%; thus, the F1 score is equal to 100%.

It is important to mention that in the macro-average approach, the contribution of all classes in the final averaged metric is equal regardless of their size in the data set. Therefore, it is useful to use it with imbalanced data to deal with and give weight to each class equally. In contrast, in the weighted-average approach, the classes' contribution in the final averaged metric is according to their size in the data set. Therefore, we can see that the macro-average and weighted-average approaches have the same score in the case of precision, recall, and F1 score. This result might be due to using the balanced data for each type of VB6Ds (54, 18, and 18 data points for the train, validation, and test, respectively), where the contribution and size of each individual of VB6Ds are equal (Table 1). Therefore, the models' performance was highlighted in all classes equally. Altogether, there is no doubt that CNN outperforms DNN. This powerful performance of CNN might be due to its ability to learn and extract remarkable features without any previous knowledge.[32,35] Additionally, the ROC curve and area under the curve have been presented in the Supporting Information (Figure S7). What is more, a comparison between principal component analysis (as an example of the traditional algorithms) and our selected deep learning model has been presented in Figure S8.

Deep Learning Model Transferring for Quantitative Analysis of Vitamin B_6 Derivatives. Generally, transfer learning refers to the approach that is used to solve a problem using information gained from a similar problem.[45] Therefore, after we successfully identified the five VB6Ds, we transferred the same DNN and CNN models for quantitative analysis. It is important to mention that there is no difference in the neural network construction, except for increasing the number of iterations to 10,000 and changing the output layer to fit with quantitative analysis (concentrations' prediction task), as shown in Figure S3. After that, the models have been trained with the same data set to fine-tune the parameters according to the required output layer (concentrations' prediction task). Of note, in this case, the data set consists of nine concentrations for five VB6Ds with 10 replicates. Figure S9 presents the training history of DNN and CNN models at 10,000 epochs. In the same manner, the best results have been considered according to our previous criteria (the lowest value of the validation loss). Accordingly, Figure 4 represents that the best results were found at 9253 and 2622 epochs for DNN and CNN models, respectively.

Figure 5 represents the linear relations between predicted and actual concentration values of five VB6Ds. It is worth knowing

https://doi.org/10.1021/acs.analchem.2c00655
Anal. Chem. 2022, 94, 9287−9296

that the presented R^2 and other metrics present the overall performance. The R^2 values indicated the satisfactory performance of the DNN model for the test set of 93.28%. As expected, the performance of the CNN model showed a better result, mainly in the test set of 97.01%. This result presents that the CNN model outperforms the DNN model. What is more, Table S1 (test set as an example) clearly shows this impression due to the presence of minus values in the concentrations prediction of the selected VB6Ds using DNN, which did not present in the concentrations' prediction results of CNN. These results emphasize the ability of CNN to extract more intrinsic information from raw spectra.[33,35]

Although some researchers presented the superiority of some metrics over others, we believed that the combination of several metrics might be better to evaluate the models' performance accurately.[61] Therefore, in Table 2, we presented five metrics for models' evaluation and comparison. As shown in Table 2, MedAE showed the lowest value in all groups than other values. This result indicated that MedAE is more robust and less affected by outliers, even lesser than MAE. Of note, the CNN model surpassed DNN by a decrease of 31, 34, and 32% of MAE in the train, validation, and test set, respectively. Furthermore, the CNN model surpassed DNN by a decrease of 35, 77, and 66% of MedAE in the train, validation, and test set, respectively. Moreover, the CNN model surpassed DNN by a decrease of 47, 13, and 55% of MSE in the train, validation, and test set, respectively. Also, the CNN model surpassed DNN by a decrease of 47, 7, and 33% of RMSE in the train, validation, and test set, respectively. The previous publications revealed that the lower value of MSE and RMSE and the higher value of R^2 led to better models' performance and accuracy.[62,63] What is more, small values of RMSE (also MSE) indicated that the obtained models are not susceptible to overfitting.[64] Thus, there may be a slight tendency for overfitting in the test set of DNN, where the values of MSE and R^2 are 81.05 and 93.28%, respectively. Altogether, these results indicate the superiority of CNN for qualitative and quantitative analysis of VB6Ds over DNN. Therefore, 3D fluorescence of Cys/NAC−AuNCs based on deep learning could be successfully applied for qualitative and quantitative analysis of VB6Ds. What is more, other statistical analyses can be found in the Supporting Information (Tables S2 and S3).

Table 2. Overall Performance Report of DNN and CNN Models for the Quantitative Analysis of the Selected VB6Ds Using 3D Fluorescence Data

dataset		MAE	MedAE	MSE	RMSE	R^2
train set	DNN	1.52	1.15	3.86	1.96	1.00
	CNN	1.05	0.74	2.02	1.42	1.00
validation set	DNN	4.18	3.41	29.65	5.45	0.98
	CNN	2.75	1.12	25.80	5.08	0.98
test set	DNN	5.18	3.34	81.05	9.00	0.93
	CNN	3.50	1.47	36.12	6.01	0.97

Furthermore, the limit of detection (LOD) of pyridoxal 5′-phosphate—as an example for the rest of VB6Ds—is presented in the Supporting Information (Figure S10). Pyridoxal 5′-phosphate is the biologically active form and acts as an enzyme cofactor and regulator for many enzymatic reactions.[14] Accordingly, we chose it in our study as an example of the LOD study. Using partial least squares regression, the LOD of pyridoxal 5′-phosphate was calculated to be 16.95 nM.[65,66] Also, the dynamic range was 0.1−100 μM. Moreover, other analytical aspects, including the applicability of our approach in real samples can be found in Table S4. Also, the effect of the mixtures of VB6Ds on the analytical performance of our proposed approach at different concentrations can be found in Table S5. Our results demonstrate that our optimized models can achieve excellent accuracy and efficiency in different applications including real samples application and multiplex detection with negligible effect on the analytical performance when using an adequate training set.

CONCLUSIONS

Altogether, a deep learning approach has been well-established based on subtle information of different 3D fluorescence spectra. The interaction of Cys/NAC−AuNCs and different VB6Ds led to varying changes in the 3D fluorescence of Cys/NAC−AuNCs. Therefore, Cys/NAC−AuNCs solution has been used as a single probe for qualitative and quantitative analysis of five VB6Ds. Our proposed deep learning-based approach is simple, fast, low-cost, and accurate, with an accuracy reach of 97.77% for the CNN model in the test set. The proposed deep learning-based approach has been transferred to solve the concentrations' prediction task with a broad concentration range (1−100 μM). It should be noted that the concentration range used (1−100 μM) is much lower than the normal intake range of vitamin B_6 (1−2 mM). Additionally, also for the quantitative analysis, the CNN model was superior to the DNN model, and the R^2 of the test set for the CNN model was 97.01%. Therefore, our results confirmed the superiority of the CNN model for the qualitative and quantitative analysis of VB6Ds. Also, issues such as LOD, real sample application, and multiplex detection have been highlighted in our study. In the future, using a single probe to build the sensor array will reduce the cost, decrease the workload, increase the accuracy, and improve the specificity. Also, the combination between deep learning algorithms and subtle fingerprint information of different 3D fluorescence spectra derived from the interaction of AuNCs and small molecules opens a new window for the qualitative and quantitative analyses of small molecules in complex media.

ASSOCIATED CONTENT

Supporting Information

The Supporting Information is available free of charge at https://pubs.acs.org/doi/10.1021/acs.analchem.2c00655.

Experimental methods, including preparation of the sensor array probe, the detection method of vitamin B_6 derivatives, 3D fluorescence data acquisition and preprocessing, and model construction and additional results, including convergence curves during the fine-tuning process in the models' training for the classification and regression task, ROC curve of the DNN and CNN models, LOD of pyridoxal 5′-phosphate, additional statistical analysis, real sample applicability, and multiplex detection ability (PDF)

AUTHOR INFORMATION

Corresponding Authors

Hao-Hua Deng − *Fujian Key Laboratory of Drug Target Discovery and Structural and Functional Research, School of Pharmacy, Fujian Medical University, Fuzhou 350004, China;* orcid.org/0000-0002-3810-0686; Email: DHH8908@163.com

https://doi.org/10.1021/acs.analchem.2c00655
Anal. Chem. 2022, 94, 9287−9296

Wei Chen − *Fujian Key Laboratory of Drug Target Discovery and Structural and Functional Research, School of Pharmacy, Fujian Medical University, Fuzhou 350004, China;* orcid.org/0000-0003-3233-8877; Phone: +86 591 22862016; Email: chenandhu@163.com

Authors

Hamada A. A. Noreldeen − *Fujian Key Laboratory of Drug Target Discovery and Structural and Functional Research, School of Pharmacy, Fujian Medical University, Fuzhou 350004, China; National Institute of Oceanography and Fisheries, NIOF, Cairo 4262110, Egypt*

Kai-Yuan Huang − *Fujian Key Laboratory of Drug Target Discovery and Structural and Functional Research, School of Pharmacy, Fujian Medical University, Fuzhou 350004, China*

Gang-Wei Wu − *Department of Pharmacy, Fujian Provincial Hospital, Fuzhou 350001, China*

Hua-Ping Peng − *Fujian Key Laboratory of Drug Target Discovery and Structural and Functional Research, School of Pharmacy, Fujian Medical University, Fuzhou 350004, China;* orcid.org/0000-0002-3357-337X

Complete contact information is available at: https://pubs.acs.org/10.1021/acs.analchem.2c00655

Notes

The authors declare no competing financial interest.

■ ACKNOWLEDGMENTS

The authors gratefully acknowledge the financial support of the National Natural Science Foundation of China (21675024 and 21804021), the Program for Innovative Leading Talents in Fujian Province (2016B016), and the Program for Innovative Research Team in Science and Technology in Fujian Province University (2018B033).

■ REFERENCES

(1) El Qaidi, S.; Yang, J.; Zhang, J.-R.; Metzger, D. W.; Bai, G. *J. Bacteriol.* **2013**, *195*, 2187−2196.
(2) Horrobin, D. F. *Am. J. Clin. Nutr.* **1993**, *57*, 732S−737S.
(3) Grogan, D. W. *Arch. Microbiol.* **1988**, *150*, 363−367.
(4) Cui, R.; Iso, H.; Date, C.; Kikuchi, S.; Tamakoshi, A. *Stroke* **2010**, *41*, 1285−1289.
(5) Bilski, P.; Li, M. Y.; Ehrenshaft, M.; Daub, M. E.; Chignell, C. F. *Photochem. Photobiol.* **2000**, *71*, 129−134.
(6) Ishihara, J.; Otani, T.; Inoue, M.; Iwasaki, M.; Sasazuki, S.; Tsugane, S.; Tsugane, S. *J. Nutr.* **2007**, *137*, 1808−1814.
(7) Nirmagustina, D. E.; Yang, Y.; Kumrungsee, T.; Yanaka, N.; Kato, N. *J. Nutr. Sci. Vitaminol.* **2018**, *64*, 116−128.
(8) Phillips, W. E. J.; Mills, J. H. L.; Charbonneau, S. M.; Tryphonas, L.; Hatina, G. V.; Zawidzka, Z.; Bryce, F. R.; Munro, I. C. *Toxicol. Appl. Pharmacol.* **1978**, *44*, 323−333.
(9) Bender, D. A. *Br. J. Nutr.* **1999**, *81*, 7−20.
(10) Schaeppi, U.; Krinke, G. *Agents Actions* **1982**, *12*, 575−582.
(11) Mori, K.; Kaido, M.; Fujishiro, K.; Inoue, N.; Koide, O. *Arch. Microbiol.* **1992**, *66*, 198−203.
(12) Tsutsumi, S.; Tanaka, T.; Gotoh, K.; Akaike, M. *J. Toxicol. Sci.* **1995**, *20*, 351−365.
(13) Thiamin, R. *Dietary Reference Intakes for Thiamin, Riboflavin, Niacin, Vitamin B6, Folate, Vitamin B12, Pantothenic Acid, Biotin, and Choline*; The National Academies Press: Washington, DC, 1998; pp 150−195.
(14) Van den Eynde, M. D. G.; Scheijen, J. L. J. M.; Stehouwer, C. D. A.; Miyata, T.; Schalkwijk, C. G. *Clin. Nutr.* **2021**, *40*, 4624−4632.
(15) Stover, P. J.; Field, M. S. *Adv. Nutr.* **2015**, *6*, 132−133.
(16) Deng, H.-H.; Shi, X. Q.; Balasubramanian, P.; Huang, K. Y.; Xu, Y. Y.; Huang, Z. N.; Peng, H. P.; Chen, W. *Nanomaterials* **2020**, *10*, 281.
(17) Zhang, X.-P.; Huang, K.-Y.; He, S.-B.; Peng, H.-P.; Xia, X.-H.; Chen, W.; Deng, H.-H. *J. Hazard. Mater.* **2021**, *405*, 124259.
(18) Wu, Y.; Wang, B.; Wang, K.; Yan, P. *Anal. Methods* **2018**, *10*, 3939−3944.
(19) Jia, T.-T.; Yang, G.; Mo, S.-J.; Wang, Z.-Y.; Li, B.-J.; Ma, W.; Guo, Y.-X.; Chen, X.; Zhao, X.; Liu, J.-Q.; Zang, S.-Q. *ACS Nano* **2019**, *13*, 8320−8328.
(20) Wang, M.; Wang, M.; Wang, G.; Su, X. *Analyst* **2020**, *145*, 1001−1007.
(21) Jiang, X.; Feng, D.-Q.; Liu, G.; Fan, D.; Wang, W. *Sens. Actuators, B* **2016**, *232*, 276−282.
(22) Huang, K.-Y.; He, H.-X.; He, S.-B.; Zhang, X.-P.; Peng, H.-P.; Lin, Z.; Deng, H.-H.; Xia, X.-H.; Chen, W. *Sens. Actuators, B* **2019**, *296*, 126656.
(23) Teng, Y.; Jia, X.; Li, J.; Wang, E. *Anal. Chem.* **2015**, *87*, 4897−4902.
(24) Han, X.; Man, Z.; Xu, S.; Cong, L.; Wang, Y.; Wang, X.; Du, Y.; Zhang, Q.; Tang, S.; Liu, Z.; Li, W. *Colloids Surf., B* **2019**, *173*, 478−485.
(25) Ma, Y.; Li, Y.; Ma, K.; Wang, Z. *Sci. China: Chem.* **2018**, *61*, 643−655.
(26) Li, Z.; Zhang, S.; Yu, T.; Dai, Z.; Wei, Q. *Anal. Chem.* **2019**, *91*, 10448−10457.
(27) Sun, S.; Jiang, K.; Qian, S.; Wang, Y.; Lin, H. *Anal. Chem.* **2017**, *89*, 5542−5548.
(28) Noreldeen, H. A. A.; Yang, L.; Guo, X.-Y.; He, S.-B.; Peng, H.-P.; Deng, H.-H.; Chen, W. *Analyst* **2022**, *147*, 101−108.
(29) He, W.; Luo, L.; Liu, Q.; Chen, Z. *Anal. Chem.* **2018**, *90*, 4770−4775.
(30) Li, Z.; Askim, J. R.; Suslick, K. S. *Chem. Rev.* **2019**, *119*, 231−292.
(31) Pandit, S.; Banerjee, T.; Srivastava, I.; Nie, S.; Pan, D. *ACS Sens.* **2019**, *4*, 2730−2737.
(32) Kabir Anaraki, A.; Ayati, M.; Kazemi, F. *Biocybern. Biomed. Eng.* **2019**, *39*, 63−74.
(33) Yu, X.; Wang, J.; Wen, S.; Yang, J.; Zhang, F. *Biosyst. Eng.* **2019**, *178*, 244−255.
(34) Liu, J.; Osadchy, M.; Ashton, L.; Foster, M.; Solomon, C. J.; Gibson, S. J. *Analyst* **2017**, *142*, 4067−4074.
(35) Yang, J.; Xu, J.; Zhang, X.; Wu, C.; Lin, T.; Ying, Y. *Anal. Chim. Acta* **2019**, *1081*, 6−17.
(36) Manak, M. S.; Varsanik, J. S.; Hogan, B. J.; Whitfield, M. J.; Su, W. R.; Joshi, N.; Steinke, N.; Min, A.; Berger, D.; Saphirstein, R. J.; Dixit, G.; Meyyappan, T.; Chu, H.-M.; Knopf, K. B.; Albala, D. M.; Sant, G. R.; Chander, A. C. *Nat. Biomed.* **2018**, *2*, 761−772.
(37) Yuan, J.; Zhao, R.; Xu, J.; Cheng, M.; Qin, Z.; Kou, X.; Fang, X. *Commun. Biol.* **2020**, *3*, 669.
(38) Xu, J.; Qin, G.; Luo, F.; Wang, L.; Zhao, R.; Li, N.; Yuan, J.; Fang, X. *J. Am. Chem. Soc.* **2019**, *141*, 6976−6985.
(39) Shi, H.; Wang, H.; Meng, X.; Chen, R.; Zhang, Y.; Su, Y.; He, Y. *Anal. Chem.* **2018**, *90*, 14216−14221.
(40) Duan, Q.; Lee, J.; Zheng, S.; Chen, J.; Luo, R.; Feng, Y.; Xu, Z. *Chem. Commun.* **2020**, *56*, 1058−1061.
(41) Ayres, L. B.; Gomez, F. J. V.; Linton, J. R.; Silva, M. F.; Garcia, C. D. *Anal. Chim. Acta* **2021**, *1161*, 338403.
(42) Lu, W.; Chen, X.; Wang, L.; Li, H.; Fu, Y. V. *Anal. Chem.* **2020**, *92*, 6288−6296.
(43) LeCun, Y.; Bengio, Y. *Handb. Brain Theory Neural Networks* **1995**, *3361*, 1995.
(44) Swati, Z. N. K.; Zhao, Q.; Kabir, M.; Ali, F.; Ali, Z.; Ahmed, S.; Lu, J. *Comput. Med. Imaging Graph.* **2019**, *75*, 34−46.
(45) Cui, F.; Yue, Y.; Zhang, Y.; Zhang, Z.; Zhou, H. S. *ACS Sens.* **2020**, *5*, 3346−3364.
(46) Deng, H.-H.; Huang, K.-Y.; He, S.-B.; Xue, L.-P.; Peng, H.-P.; Zha, D.-J.; Sun, W.-M.; Xia, X.-H.; Chen, W. *Anal. Chem.* **2020**, *92*, 2019−2026.
(47) Hassan, D. S.; Wolf, C. *Nat. Commun.* **2021**, *12*, 6451.

(48) Géron, A. *Hands-on Machine Learning with Scikit-Learn, Keras, and TensorFlow: Concepts, Tools, and Techniques to Build Intelligent Systems*; O'Reilly Media, 2019.
(49) Noreldeen, H. A. A.; Liu, X.; Wang, X.; Fu, Y.; Li, Z.; Lu, X.; Zhao, C.; Xu, G. *Int. J. Mass Spectrom.* **2018**, *434*, 172−178.
(50) Cho, S.-Y.; Lee, Y.; Lee, S.; Kang, H.; Kim, J.; Choi, J.; Ryu, J.; Joo, H.; Jung, H.-T.; Kim, J. *Anal. Chem.* **2020**, *92*, 6529−6537.
(51) Fairbairn, C. E.; Kang, D.; Bosch, N. *Drug Alcohol Depend.* **2020**, *216*, 108205.
(52) Bonnin, R. *Machine Learning for Developers: Uplift Your Regular Applications with the Power of Statistics, Analytics, and Machine Learning*; Packt Publishing Ltd., 2017.
(53) Nagelkerke, N. J. D. *Biometrika* **1991**, *78*, 691−692.
(54) Ju, L.; Lyu, A.; Hao, H.; Shen, W.; Cui, H. *Anal. Chem.* **2019**, *91*, 9343−9347.
(55) Zhang, X.; Lin, T.; Xu, J.; Luo, X.; Ying, Y. *Anal. Chim. Acta* **2019**, *1058*, 48−57.
(56) Cui, C.; Fearn, T. *Chemom. Intell. Lab. Syst.* **2018**, *182*, 9−20.
(57) Ni, C.; Wang, D.; Tao, Y. *Spectrochim. Acta, Part A* **2019**, *209*, 32−39.
(58) Padarian, J.; Minasny, B.; McBratney, A. B. *Geoderma Reg.* **2019**, *16*, No. e00198.
(59) Wang, Y.; Sun, L.; Subramani, S. *KSII Trans. Internet Inf. Syst.* **2021**, *15*, 2304−2320.
(60) Li, Z.; Askim, J. R.; Suslick, K. S. *Chem. Rev.* **2018**, *119*, 231−292.
(61) Chai, T.; Draxler, R. R. *Geosci. Model Dev.* **2014**, *7*, 1247−1250.
(62) Massah, J.; Asefpour Vakilian, K. *Biosyst. Eng.* **2019**, *177*, 49−58.
(63) Jiang, S.; Wang, J.; Wang, Y.; Cheng, S. *Sens. Actuators, B* **2017**, *242*, 511−521.
(64) Głowacz, K.; Drozd, M.; Ciosek-Skibińska, P. *Mikrochim. Acta* **2021**, *188*, 343.
(65) Goicoechea, H. C.; Olivieri, A. C. *Anal. Chem.* **1999**, *71*, 4361−4368.
(66) Olivieri, A. C. *Chem. Rev.* **2014**, *114*, 5358−5378.

https://doi.org/10.1021/acs.analchem.2c00655
Anal. Chem. 2022, 94, 9287−9296